Combined Effect of Surface Roughness and Magnetohydrodynamic with Micropolar Fluid between Porous Triangular Plates

M. Faizan Ahmed and E. Sujatha

***Abstract*—This paper aims to study the combined effect of surface roughness and magnetohydrodynamic (MHD) on triangular plates with squeeze film characteristics. Using Christensen's theory, the modified stochastic Reynold's equation for the one-dimensional structure of the azimuthal and radial roughness patterns is obtained. Micropolar fluid is used as the lubricant for the considered case. The solution is obtained analytically for mean squeeze film pressure and workload. The results obtained by comparing the MHD with non-MHD situations shows that the presence of MHD enhances the pressure and workload. Further, it is seen that as the roughness parameter increases, the pressure and workload increase with distance and height, respectively. An increase in the values of coupling number, Hartmann number and roughness parameter increase the squeeze time of the lubricant.**

***Index Terms*—Micropolar fluid, MHD, porosity, surface roughness, triangular plates.**

I. Introduction

SQUEEZE film technology has several applications in various industries, from very small parts of the machinery that involve disc clutches to huge power plants that employ turbo machinery, all of which may have specific rotating devices where the lubricant is squeezed into the system to lubricate the rotating parts. With the advancement of modern machine tools, the application of non-Newtonian fluids has increased. The outcome of a recent experiment reveals that when the base oil is combined with long-chained additives, it enhances the lubricating capabilities of the system, further decreasing friction and intern the damage caused to the surface of interaction. The rheological characteristics of non-Newtonian fluids have been analyzed using several micro continuum theory models. The micro-rotational and inertia due to the rotation of the microparticles makes micropolar fluid (MPF) stand out as a unique non-Newtonian fluid. Erigen [5] laid down the basis for MPF's micro continuum theory. Numerous studies applying this theory have analyzed the squeezing flow in various geometric structures. Prakash and Sinha [15] studied the effect of MPF on parallel plates. Sinha and Singh [21] studied the impact of MPF on hemispherical bearings. Siddangouda [20] analyzed the same for parallel stepped plates. These works bring out the fact that the application of the MPF as a lubricant increases the load capacity.

The movement of an object when acted upon by force is referred to as dynamics. When this movement is considered for a fluid particle in the presence of a magnetic fluid, the concept is referred to as magnetohydrodynamics (MHD). Hartmann first took up the initial work on MHD flow and its characteristics, where a magnetic field of strength B_0 was applied in a direction normal to the fluid flow. He studied its effect theoretically and experimentally when applied to an incompressible fluid between parallel planes. Thus the flow of such kind is referred to as Hartmann flow. A lot of theoretical and analytical research work has been carried out in recent years based on MHD flows theory have been published in recent years Anncy et al. [1], Salah et al. [19], Elniel et al. [4], Nayak [12], Cowling [3], M. Hamza [7], Kuzma [11], Sujatha and Sundarammal [22], Toloian et al. [23], Fathima et al. [6], Patel et al. [16] and many more found that the electromagnetic forces due to the application of MHD made the load carrying capacity much better than the non-magnetic case.

As the machines operate longer, the interaction of the additives in the lubricant, which adds additives to enhance the lubricating properties, converts a Newtonian fluid into a non-Newtonian liquid. This constant interaction leads to chemical and physical changes to the surface which comes into contact with the fluid. When these changes are neglected, they may cause more significant damage to the machine parts due to wear and tear. Researchers have started focusing on this subject to investigate the lubricant's impact on a surface texture. Christensen [2] developed a stochastic model to examine the impact of roughness on bearing performance. Prakash and Tonder [17], Naduvinamani and Siddangouda [13], Vadher [24], Rao et al. [18], Hanumagowda et al. [8] made a detailed study on the effect caused by the wearing of the machine parts due to the interaction of the lubricant with the surface of various geometrical structures. Much research has been done on MHD lubrication for smooth and rough bearing surfaces. Halambi et al. [9] analyzed with rough, porous elliptic plates, Hanumagowda [10] studied the impacts on a rough flat plate and curved annular plates, Naduvinamani [14] analyzed with porous circular stepped plates. According to their conclusions, MHD and surface roughness significantly improve the load-carrying capacity.

The motivation for this article was drawn from wet clutches, which are used to cool the clutch pack over which the lubricant flows through. These wet clutches have grooves on their surface, which are triangular in form. The squeeze film action between triangular plate can also be found in other machinery actions. This inspired to take up the work on

Manuscript received Jan 28 2023; revised Oct 4 2023.

M. Faizan Ahmed is a Research Scholar in the Department of Mathematics, College of Engineering and Technology, SRM Institute of Science and Technology, Kattankulathur 603203, Tamil Nadu, India (e-mail: fm0834@srmist.edu.in).

E. Sujatha is an Assistant Professor in the Department of Mathematics, College of Engineering and Technology, SRM Institute of Science and Technology, Kattankulathur 603203, Tamil Nadu, India (Corresponding author; phone:9884708590; e-mail: sujathae@srmist.edu.in).

squeeze film lubrication between triangular plate by applying an external magnetic field when lubricated with MPF. The impact of surface roughness on such a surface kindled the interest in investigating this model.

II. Geometry of the Bearing

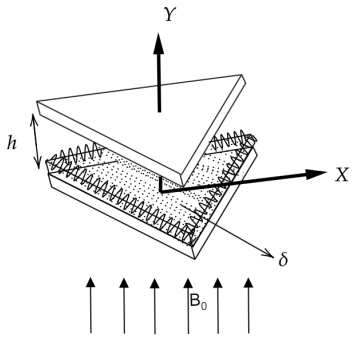

Fig. 1: Geometry of the Bearing

Fig. 1 depicts the geometry of the triangular plates that are lubricated with micropolar fluid. The gap between the upper and the lower plate is filled with the micropolar fluid. The thickness of this fluid is considered as h. The bottom plate is oriented towards the x axis and remains fixed. The upper plate moves towards the lower plate with a normal velocity $v = \frac{d(2h)}{dt}$. The lower plate is considered to be porous with thickness δ and it is supported below by a solid backing. Also, the lower surface is assumed to be rough, which adds to the surface roughness asperities, which can be expressed mathematically by the form,

$$H = h\,(t) + h_s(x, y, \zeta)$$

The first part of the above expression represents the deterministic part of the film thickness and the second part represents the random part of the film thickness. ζ is the index parameter that determines the exact roughness pattern.

The expectancy operator $E(\star)$ is given by

$$E\,(\star) = \int_{-\infty}^{\infty} (\star) f(h_s) ds$$

where $f(h_s)$ is the probability density function of the stochastic variable h_s and is expressed as,

$$f(h_s) = \begin{cases} \frac{35}{32c^7}(c^2 - h_s^2)^3, & -c < h_s < c. \\ 0, & \text{otherwise.} \end{cases}$$

III. MATHEMATICAL FORMULATION

The basic assumptions of thin film lubrication for a micropolar fluid as described by Eringen [1] is assumed to hold true for the case discussed here. The following equations are considered for deriving the expression for velocity.

$$\left(\mu + \frac{\chi}{2}\right)\frac{\partial^2 u}{\partial y^2} + \chi\frac{\partial v_2}{\partial y} - \sigma B_0^2 u = -\frac{\partial p}{\partial x} \tag{1}$$

$$\gamma\frac{\partial^2 v_2}{\partial y^2} - 2\chi v_2 - \chi\frac{\partial u}{\partial y} = 0 \tag{2}$$

$$\frac{\partial p}{\partial y} = 0 \tag{3}$$

$$\frac{\partial u}{\partial x} + \frac{\partial v}{\partial y} = 0 \tag{4}$$

Equation (1), (2) and (4) represents conservation of linear momentum, conservation of angular momentum and conservation of mass, respectively. (u, v) represents velocity components in the directions (x, y). v_2 represents the velocity component of micro-rotation, p represents film pressure, σ represents electrical conductivity of the fluid, γ denotes the viscosity co-efficient of micropolar fluid, χ denotes the spin viscosity, μ indicates the Newtonian viscosity and B_0 denotes the magnetic field strength.

The boundary conditions (B.C) applicable for the above situation are;

For the upper plate $(y = h)$

$$u = v_2 = 0,\ v = \frac{d(2h)}{dt} \tag{5}$$

For the lower plate $(y = -h)$

$$u = v_2 = 0,\ v = v^\star \tag{6}$$

By solving equations (1) and (2) and applying B.C's (5) and (6), the expression for the velocity component u is given by

$$u = -\frac{\frac{\partial p}{\partial x}\begin{bmatrix}\omega_2 sinh(r_2 h)[cosh(r_1 h) - cosh(r_1 y)] \\ -\omega_1 sinh(r_1 h)[cosh(r_2 h) - cosh(r_2 y)]\end{bmatrix}}{\sigma B_0^2\begin{bmatrix}\omega_2 sinh(r_2 h) cosh(r_1 h) - \\ \omega_1 sinh(r_1 h) cosh(r_2 h)\end{bmatrix}} \tag{7}$$

The nature of the flow of fluid through the porous medium was first described by Darcy who gave the expression for the velocity component $(q^\star)$ in the porous medium as

$$q^\star = -\frac{k}{(\mu + \chi)}\nabla p^\star \tag{8}$$

Here $p^\star$ denotes the pressure in porous region and k represents permeability. The continuity equation in the porous region is given by

$$\frac{\partial^2 p^\star}{\partial x^2} + \frac{\partial^2 p^\star}{\partial y^2} = 0 \tag{9}$$

The component of velocity $v^\star$ at $y = -h$ (lower surface) is obtained as,

$$(v^\star)_{y=-h} = \left(\frac{k\delta}{\mu + \chi}\right)\left(\frac{\partial^2 p}{\partial x^2}\right) \tag{10}$$

The continuity equation (4) along with B.C's (5) and (6) leads to the modified Reynold's equation which is given by

$$\frac{\partial^2 p}{\partial x^2}\left[R(h, M, L, N) + \frac{k\delta}{(\mu + \chi)}\right] = -12\frac{dh}{dt} \tag{11}$$

where

$$R(h, M, L, N) = \frac{(\Upsilon_1 - \Upsilon_2)}{\sigma B_0^2 r_1 r_2 (\Upsilon_3)} \tag{12}$$

$$\Upsilon_1 = r_2\omega_2 sinh(r_2 h)[cosh(r_1 h) r_1 - sinh(r_1 h)]$$
$$\Upsilon_2 = r_1\omega_1 sinh(r_1 h)[cosh(r_2 h) r_2 - sinh(r_2 h)]$$
$$\Upsilon_3 = \omega_2 sinh(r_2 h) cosh(r_1 h) - \omega_1 sinh(r_1 h) cosh(r_2 h)$$

$$r_1 = \left(\frac{\lambda_1 + \sqrt{\lambda_1^2 - 4\lambda_2}}{2}\right)^{1/2},\ r_2 = \left(\frac{\lambda_1 - \sqrt{\lambda_1^2 - 4\lambda_2}}{2}\right)^{1/2}$$

$$\omega_1 = \frac{2\sigma B_0^2 - (2\mu+\chi)r_1^2}{2\chi r_1},\ \omega_2 = \frac{2\sigma B_0^2 - (2\mu+\chi)r_2^2}{2\chi r_2},$$

$$\lambda_1 = \frac{4\mu\chi + 2\gamma\sigma B_0^2}{\gamma(2\mu+\chi)},\ \lambda_2 = \frac{4\chi\sigma B_0^2}{\gamma(2\mu+\chi)}$$

Dimensionless form of the modified Reynold's equation is given by

$$\frac{\partial^2 p}{\partial x^2}\left[R^\star(H^\star, M, L, N, \Psi)\right] = -12 \tag{13}$$

The stochastic average of equation (13) is obtained by applying expectation operation on both sides of (13) with respect to $f(h_s)$, which takes the form

$$\frac{\partial^2 E(p)}{\partial x^2}\left[E(R^\star(H^\star, M, L, N, \Psi))\right] = -12 \tag{14}$$

Equation (14) represents the average modified Reynolds equation for radial roughness pattern.

$$\frac{\partial^2 E(p)}{\partial x^2}\left[\frac{1}{E\left(\frac{1}{R^\star(H^\star, M, L, N, \Psi)}\right)}\right] = -12 \tag{15}$$

Equation (15) represents the average modified Reynolds equation for azimuthal roughness pattern.

Both the roughness patterns, namely radial and azimuthal, are generally oriented in the direction of x and y, respectively. In this article, radial roughness is considered to be a one-dimensional roughness structure. The values for the azimuthal roughness can be obtained similar to the radial roughness by rotating the coordinate axes suitably.

Here

$$R^\star(H^\star, M, L, N, \Psi) = \frac{24(G_1 - G_2)}{\sigma B_0^2 \tilde{r_1}\tilde{r_2}(G_3 - G_4) + \left(12\Psi\left(\frac{1-N^2}{1+N^2}\right)\right)}$$

$$G_1 = \tilde{r_2}\Phi_2 sinh(0.5\tilde{r_2}H^\star)$$
$$[cosh(0.5\tilde{r_1}H^\star)0.5\tilde{r_1}H^\star - sinh(0.5\tilde{r_1}H^\star)]$$
$$G_2 = \tilde{r_1}\Phi_1 sinh(0.5\tilde{r_1}H^\star)$$
$$[cosh(0.5\tilde{r_2}H^\star)0.5\tilde{r_2}H^\star - sinh(0.5\tilde{r_2}H^\star)]$$

$$G_3 = \Phi_2 sinh(0.5\tilde{r_2}H^\star)cosh(0.5\tilde{r_1}H^\star)$$
$$G_4 = \Phi_1 sinh(0.5\tilde{r_1}H^\star)cosh(0.5\tilde{r_2}H^\star)$$

$$\tilde{r_1} = r_1 H_0 = \left(\frac{{\lambda_1}^\star + \sqrt{{\lambda_1}^{\star 2} - 4\lambda_2^\star}}{2}\right)^{1/2},$$

$$\tilde{r_2} = r_2 H_0 = \left(\frac{{\lambda_1}^\star - \sqrt{{\lambda_1}^{\star 2} - 4\lambda_2^\star}}{2}\right)^{1/2},$$

$$\lambda_1^\star = \lambda_1 H_0^2 = \frac{N^2 + M^2(1-N^2)L^2}{L^2},\ \lambda_2^\star = \lambda_2 H_0^2 = \frac{N^2 M^2}{L^2},$$

$$\omega_1^\star = \omega_1 H_0 = \frac{M^2(1-N^2) - \widetilde{r_1^2}}{2N^2\widetilde{r_1^2}},$$

$$\omega_2^\star = \omega_2 H_0 = \frac{M^2(1-N^2) - \widetilde{r_2^2}}{2N^2\widetilde{r_2^2}},$$

$$N = \left(\frac{\chi}{2\mu+\chi}\right)^{\frac{1}{2}},\ L = \frac{\left(\frac{\chi}{4\mu}\right)^{\frac{1}{2}}}{H_0},\ M = B_0 H_0\left(\frac{\sigma}{\mu}\right)^{\frac{1}{2}}$$

Where the dimensionless variables are used in the above expressions are

$$x^\star = \frac{x}{A},\ H^\star = h^\star + h_s,\ h^\star = \frac{h}{h_0} = \frac{2h}{H_0},\ \lambda_1^\star = \lambda_1 H_0^2,\ \lambda_2^\star = \lambda_2 H_0^4,$$

$$r_1^\star = r_1 H_0,\ r_2^\star = r_2 H_0,\ \omega_1^\star = \omega_1 H_0,\ \omega_2^\star = \omega_2 H_0,\ \Psi = \frac{k\delta}{H_0^3}$$

Combining equation (14) and equation (15) gives

$$\frac{\partial^2 E(p)}{\partial x^2}\left[S(H^\star, M, L, N, \Psi, c)\right] = -12 \tag{16}$$

where

$$S(H^\star, M, L, N, \Psi, c) = \begin{cases} E\left(R^\star\left(H^\star, M, L, N, \Psi\right)\right) \\ E\left(\frac{1}{R^\star(H^\star, M, L, N, \Psi)}\right)^{-1} \end{cases}$$

The pressure boundary conditions for a triangular plate are as follows $p(x', y') = 0$
where

$$(x' - a)(x' - \sqrt{3y'} + 2a)(x' + \sqrt{3y'} + 2a) = 0$$

a is the length of the equilateral triangle whose equation is

$$(x - a)\left(x - \sqrt{3y} + 2a\right)\left(x + \sqrt{3y} + 2a\right) = 0.$$

The pressure in the dimensionless form is obtained as

$$P^\star = \frac{4}{3\sqrt{3}}\left[\frac{(1-x)\left(1 - \frac{\sqrt{3y}}{2} + \frac{x}{2}\right)\left(1 + \frac{\sqrt{3y}}{2} + \frac{x}{2}\right)}{S(H^\star, M, L, N, \Psi, c)}\right] \tag{17}$$

The expected workload is obtained by

$$E\left(w\right) = \int_{-2a}^{a}\int_{\frac{-2a+x}{\sqrt{3}}}^{\frac{2a+x}{\sqrt{3}}} E(p)dydx$$

The workload in the non-dimensionless form is given by,

$$W^\star = \frac{E(w)h_0^3}{27\mu h_0 a^2} = \frac{\sqrt{3}}{5}\left[\frac{1}{S(H^\star, M, L, N, \Psi, c)}\right] \tag{18}$$

The expression for the time-height relation in the dimensionless form is given by,

$$T^\star = -\frac{E(w)h_0^2 dt}{27\mu a^2} = \frac{\sqrt{3}}{5}\int_{H_1^\star}^{1}\frac{dH^*}{S(H^\star, M, L, N, \Psi, c)} \tag{19}$$

IV. Results and Discussion

This article studies about a pair of triangular plates that squeezes out the micropolar fluid present between them as they approach each other in the presence of MHD. The effects of porosity and surface roughness are given due interest while analyzing the effects of MHD. The coupling number N and length L, which characterize the contact between fluid clearance, are two dimensionless characteristics that describes the nature of the micropolar fluid. Comparison is made between the effect created by the presence and the absence of magnetic field M. The effect of porosity Ψ and the surface roughness parameter c on the triangular plates are also analyzed and discussed below. The effect produced by the presence and absence of MHD and roughness has been brought out both using graphs and tables.
Instead of carrying out the research work for analyzing the MHD effect separately and roughness effect separately, as usually done by researches, this paper aims to consider both these effects together. The interdependence of these two effects in pressure, workload and time height has been brought out by the graphs and tables. Hence an ideal situation of working of the bearing is considered for the analysis and the results are etched.

A. Squeeze Pressure

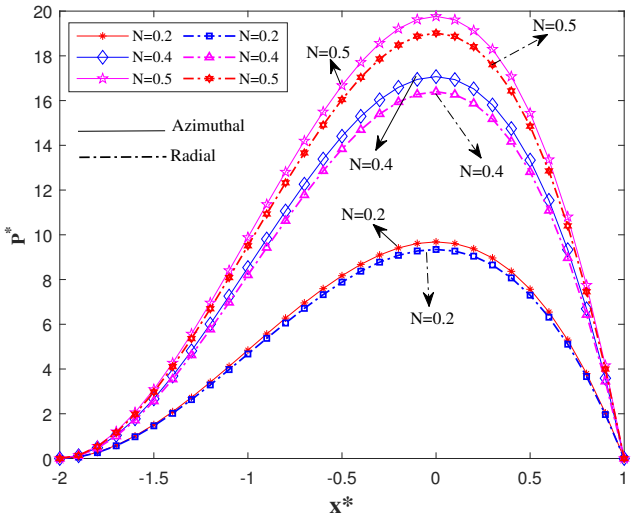

Fig. 2: Plot of pressure of with distance for coupling number $\boldsymbol{N}$

Fig. 2 shows a plot of pressure versus distance for different values of N with fixed values of M= 5, L= 0.15, c= 0.3 and Ψ= 0.001. The graph demonstrates that a non-Newtonian micropolar fluid creates additional resistance to the lubricant flow, leading to a significant increase in the pressure distribution within the fluid film region. Fig. 3 illustrates the variation of pressure with distance for different Hartmann numbers (M) with N= 0.5, L= 0.15, Ψ= 0.001 and c= 0.3. The graph clearly shows that pressure increases with increasing values of M.

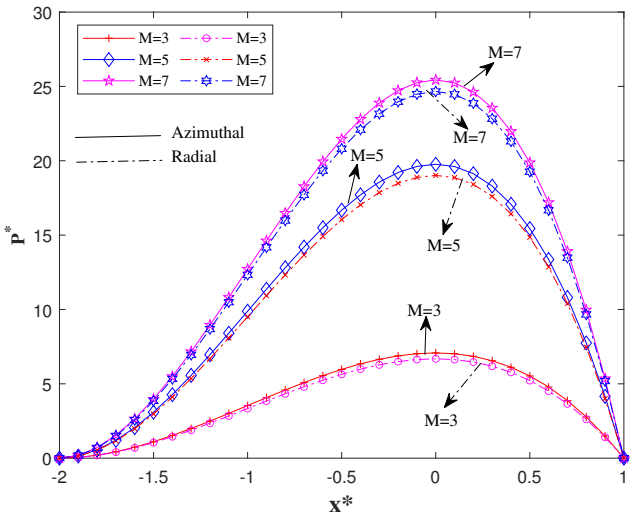

Fig. 3: Plot of pressure of with $x^{\star}$ for Hartmann number M.

Fig. 4 plots the variation of pressure with height for L= 0.15, M= 5, N= 0.5, and Ψ= 0.001, where the graph indicates that pressure rises with increasing values of c. These results highlight the significant role played by surface roughness and an externally applied magnetic field. The surface roughness and magnetic field which is applied affects the micro rotational effect of fluid particles and slows down its motion. This drop in fluid velocity allows the lubricant to stay between the plates and also in the ridges of the rough surface for prolonged time. This in turn causes a uniform rise in the pressure distribution between the plates whose change with respect to M and c have been brought out through Fig. 3 and Fig. 4.

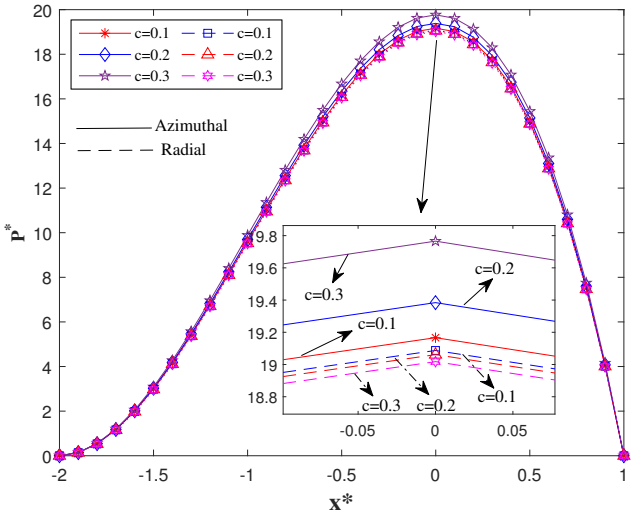

Fig. 4: Plot of pressure of with distance for roughness $\boldsymbol{c}$

B. Workload

Fig. 5 depicts a plot of workload vs. height for various values of coupling number N with the following parameters: M= 5, L= 0.15, c= 0.3 and Ψ= 0.001. The graph demonstrates that the amount of workload rises as the coupling number N rises.

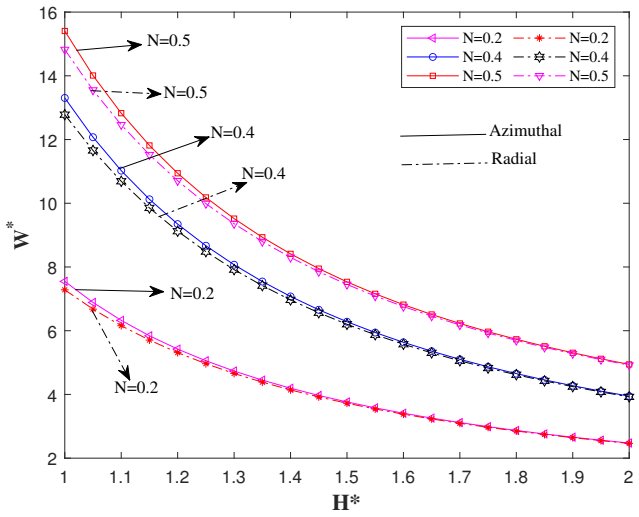

Fig. 5: Plot of workload with height for coupling number N

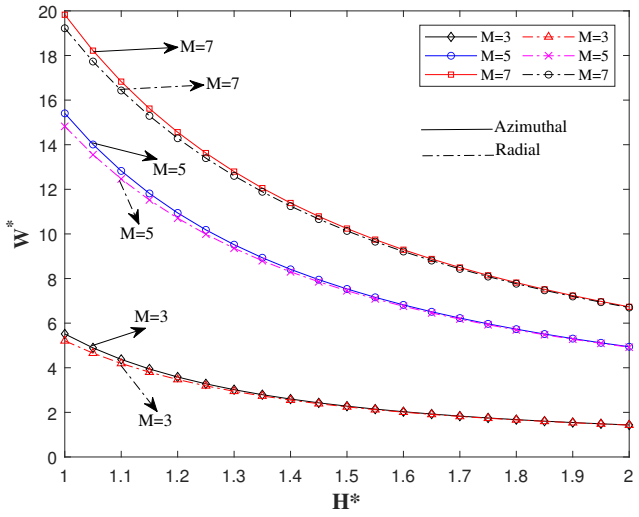

Fig. 6: A variation of workload with height for Hartmann number M

Fig. 6 depicts the workload variations with height for different values of the Hartmann constant M, when L= 0.15, Ψ= 0.001, N= 0.5. It is clear from the graph that when M is increased, so does the workload. Fig. 7 depicts the relationship between workload and height for different values of c when M= 5, N= 0.5 and Ψ= 0.01. Magnetic and non-magnetic cases with varied roughness parameters (c = 0.1, 0.2 and 0.3) are compared. For identical values of c, the magnetic case has a higher load bearing than the non-magnetic case in the same scenario. The rise in pressure between the plates over the entire fluid region creates a balanced load carrying capacity which increases with the related parameters of observation.

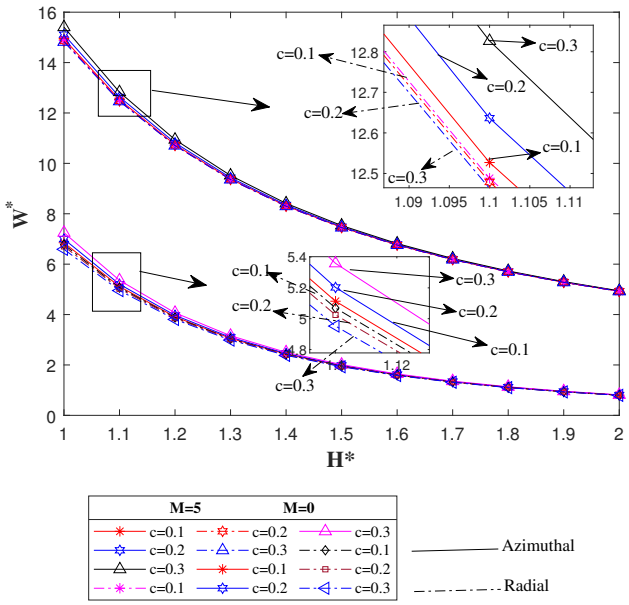

Fig. 7: A plot of workload with height for roughness parameter c

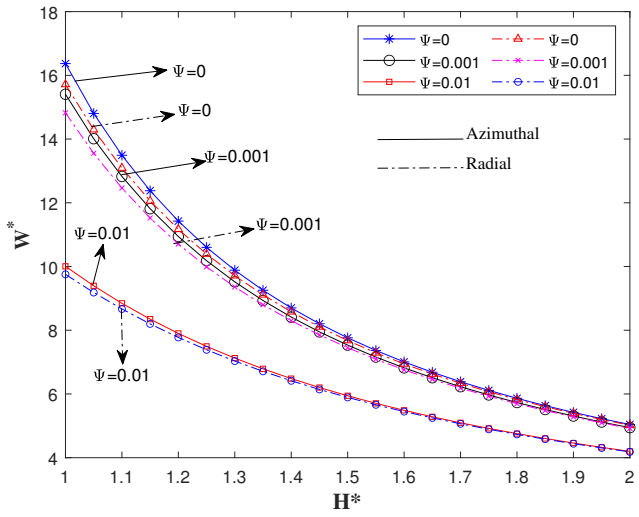

Fig. 8: A variation of workload with height for Ψ

Fig. 8 displays a plot of workload vs. height for varying values of Ψ for the parameters N= 0.5, M= 5, c= 0.3, L= 0.15, making it evident that the porosity of the material greatly reduces the workload of the bearing in contrast to the solid case. This is because porosity reduces pressure due to the pores on the porous surface acting as a pathway for lubricant flow, which decreases the amount of lubricant in the film region. Consequently, pressure build-up decreases, resulting in a decrease in the load-carrying capacity. A suitable selection of micro-structure additives added to the lubricant can overcome this adverse effect of the porosity. A plot of workload with height for different values of L with N= 0.5, M= 5, c= 0.3, Ψ = 0.001 is shown in figure 9. The graph shows that the workload increases with an increase in L.

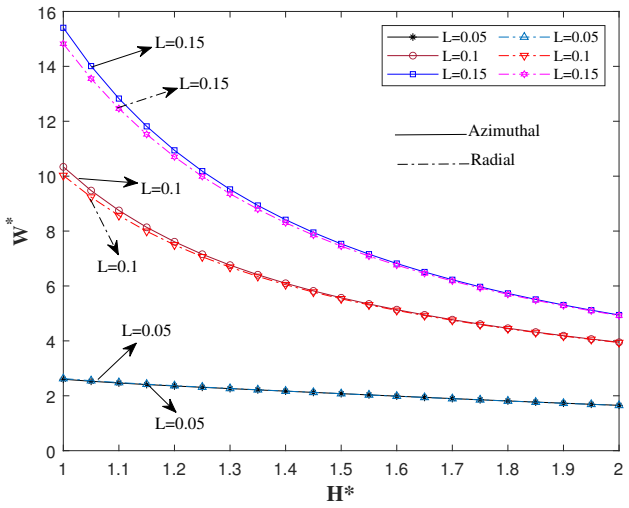

Fig. 9: A plot of workload with height for $\boldsymbol{L}$

TABLE I: Work load with and without surface roughness and MHD with $N = 0.5$, $L = 0.15$ and $\Psi = 0.001$.

With and Without MHD	Work Load: Without Rough	With Roughness: Azimuthal			Radial		
	c=0	c=0.1	c=0.2	c=0.3	c=0.1	c=0.2	c=0.3
M=5	14.296	14.938	15.108	15.405	14.876	14.856	14.822
	12.000	12.526	12.636	12.826	12.488	12.478	12.463
	10.308	10.741	10.814	10.941	10.715	10.711	10.704
	9.021	9.379	9.43	9.518	9.362	9.36	9.357
	8.016	8.313	8.35	8.412	8.301	8.301	8.3
M=0	6.801	6.849	6.993	7.249	6.778	6.706	6.591
	5.084	5.113	5.203	5.359	5.069	5.025	4.952
	3.893	3.912	3.970	4.070	3.884	3.855	3.807
	3.043	3.056	3.094	3.160	3.037	3.017	2.986
	2.421	2.430	2.456	2.501	2.417	2.403	2.381

Table I shows the variation of workload with height, comparing the presence and absence of MHD (M) and surface roughness (c). The data reveals that the presence of MHD and surface roughness enhances the workload compared to the absence of MHD and roughness.

TABLE II: Work load with presence and absence of surface roughness and porosity with $N = 0.5$, $L = 0.15$ and $M = 5$.

Surface roughness	Ψ= 0		Ψ= 0.001		Ψ= 0.01	
	Azimuthal	Radial	Azimuthal	Radial	Azimuthal	Radial
c=0.3	16.368	15.714	15.405	14.822	10.006	9.753
	14.804	14.296	14.009	13.552	9.395	9.184
	13.491	13.091	12.826	12.463	8.845	8.667
	12.378	12.059	11.814	11.522	8.348	8.199
	11.424	11.167	10.941	10.704	7.9	7.773
c=0	15.781		14.883		9.782	
	14.341		13.593		9.205	
	13.121		12.491		8.683	
	12.079		11.541		8.21	
	11.18		10.717		7.781	

Table II presents workload data against height for various values of Ψ, clearly demonstrating that the presence of porosity significantly diminishes the bearing's workload when compared to a solid case. This reduction occurs because porosity facilitates the reduction of pressure through the pores on the porous surface, acting as a pathway for lubricant flow. As a result, the quantity of lubricant in the film region decreases, leading to a decrease in pressure build-up and ultimately a reduction in load-carrying capacity.

C. Squeeze film time

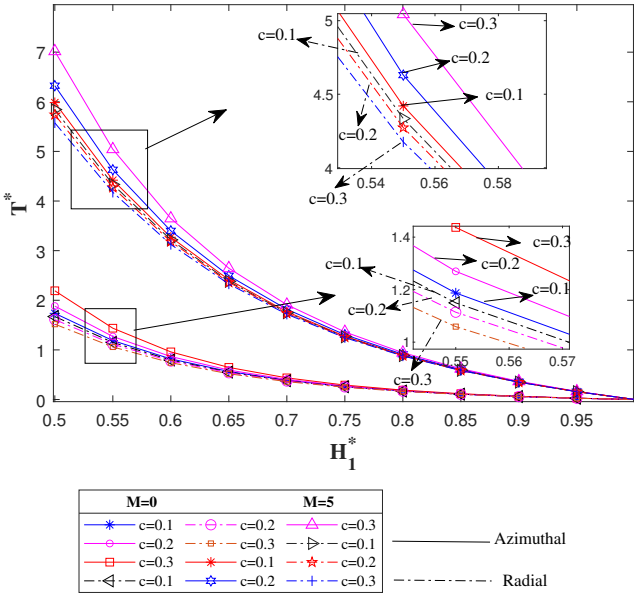

Fig. 10: A plot of time-height with $H_1^\star$ for roughness parameter $\boldsymbol{c}$

The relationship between the squeeze film time and $H_1^\star$ for different values of c is depicted in Fig. 10. The graph illustrates the comparison when $N = 0.5$ and $\Psi = 0.01$ in the presence and absence of MHD, with $M = 5$ and $M = 0$ respectively. From the graph, it is observed that the presence of MHD enhances the squeeze film time compared to the non-MHD case. The fluid settles in the ridges and valleys of the rough surface of the plate, providing an increased cushioning effect to the lubricant. Hence compared with the smooth surfaces, the rough surfaces provides a longer squeeze time. Fig. 10 brings out this result.

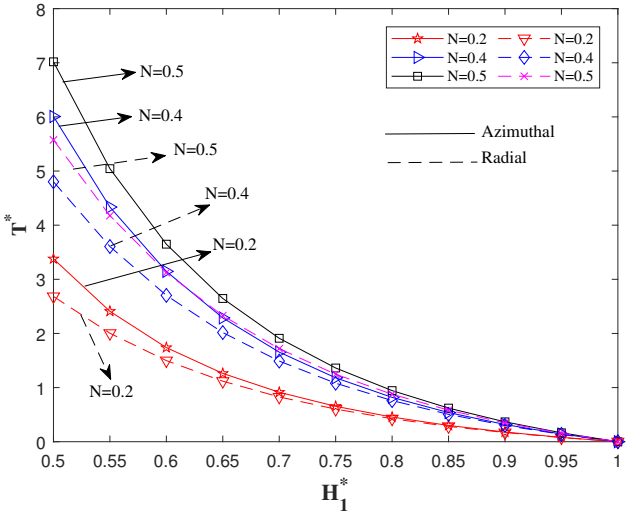

Fig. 11: Plot of time-height with $H_1^\star$ for coupling number $\boldsymbol{N}$

Fig. 11 depicts a plot of squeeze time vs. $H_1^\star$ for various values of coupling number N with the following parameters:

M= 5, L= 0.15, c= 0.3 and Ψ= 0.001. The viscosity of the fluid increase the time taken by the lubricant to get squeeze out the thickness the lubricant the longer the time of squeeze. This is clearly depicted by the Fig. 11.

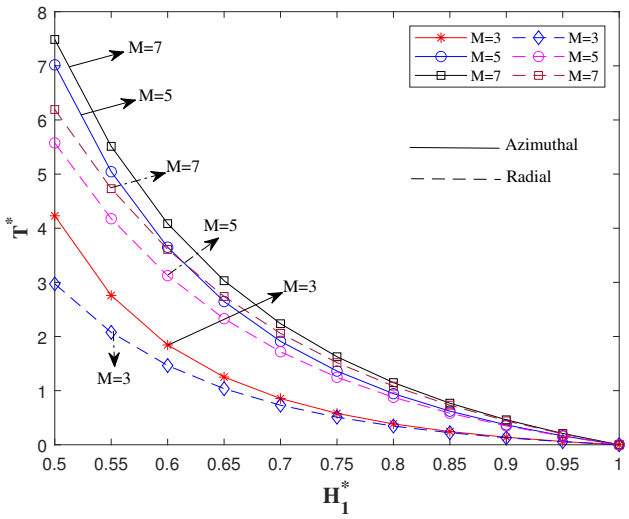

Fig. 12: A variation of squeeze time with $H_1^\star$ for Hartmann number $\boldsymbol{M}$

Fig. 12 is the plot of time-height with $H_1^\star$ for different values of the Hartmann constant M with L= 0.15, Ψ= 0.001, N= 0.5. The magnetic force applied externally helps the particles of the lubricant to retain its position for an extended period of time. This increase the squeeze time of the lubricant. This is brought out by Fig. 12. Fig. 13 is the plot of time-height vs. $H_1^\star$ for distinct values of L with M= 5, N= 0.5, c= 0.3 and Ψ= 0.001. An increase in the clearance length(L) causes an increase in squeeze time as the extra length provided by the clearance takes a little extra time to squeeze out the lubricant present between them. This is brought out through Fig. 13.

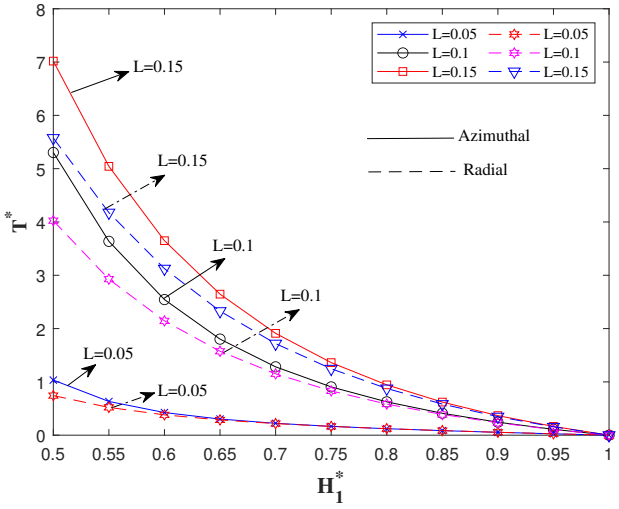

Fig. 13: A variation of squeeze time with $H_1^\star$ for $\boldsymbol{L}$

Fig. 14 illustrates graphs that reveal the influence of porosity, represented by the parameter Ψ, on the squeezing duration. It is evident from the graphs that an increase in the permeability parameter Ψ leads to a reduction in the squeezing duration. Furthermore, as the permeability parameter Ψ increases, the squeezing time consistently decreases.

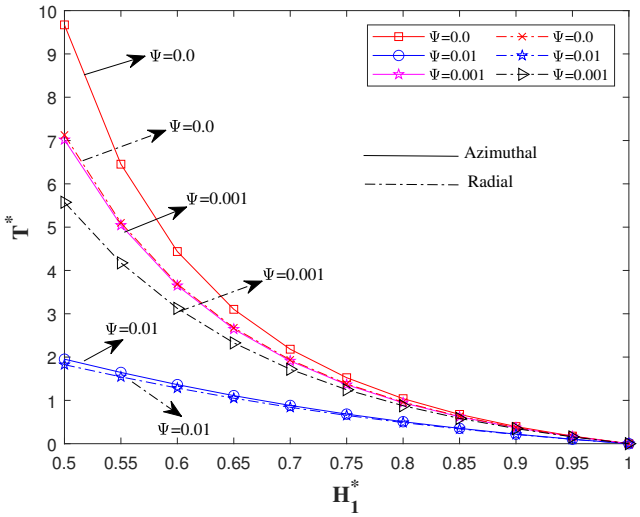

Fig. 14: A variation of squeeze time with $H_1^\star$ for $\boldsymbol{\Psi}$

TABLE III: Squeeze film time with and without surface roughness and MHD with N = 0.5, L= 0.15 and Ψ= 0.001.

Time height							
With and Without MHD	Without Rough	With Roughness					
		Azimuthal			Radial		
	c=0	c=0.1	c=0.2	c=0.3	c=0.1	c=0.2	c=0.3
M=5	5.880	5.983	6.324	7.018	5.844	5.739	5.575
	4.356	4.420	4.630	5.044	4.335	4.273	4.176
	3.230	3.270	3.400	3.649	3.217	3.182	3.124
	2.389	2.414	2.494	2.646	2.382	2.361	2.328
	1.753	1.769	1.819	1.911	1.749	1.737	1.718
M=0	1.693	1.737	1.882	2.191	1.672	1.611	1.518
	1.162	1.187	1.270	1.437	1.150	1.114	1.059
	0.803	0.818	0.866	0.960	0.796	0.775	0.742
	0.556	0.565	0.593	0.647	0.552	0.539	0.519
	0.383	0.388	0.405	0.436	0.380	0.373	0.360

Table III displays the relationship between time height and $H_1^\star$, along with a comparison of scenarios involving the presence and absence of MHD (M) and surface roughness (c). The data unequivocally shows that the combination of MHD and surface roughness leads to an increase in squeeze film time compared to the cases where MHD and roughness are absent.

TABLE IV: Squeeze film time with and without surface roughness and porosity with N = 0.5, L= 0.15 and M= 5.

Surface roughness	Ψ= 0		Ψ= 0.001		Ψ= 0.01	
	Azimuthal	Radial	Azimuthal	Radial	Azimuthal	Radial
c=0.3	9.67	7.127	7.017	5.574	1.951	1.824
	6.453	5.099	5.043	4.175	1.645	1.543
	4.436	3.686	3.648	3.124	1.363	1.284
	3.102	2.675	2.645	2.327	1.109	1.05
	2.181	1.935	1.91	1.718	0.883	0.839
c=0	7.629		5.879		1.855	
	5.367		4.355		1.566	
	3.832		3.229		1.302	
	2.755		2.388		1.062	
	1.979		1.753		0.848	

The data in Table IV reveal that with an increase in film height, the duration of the squeezing process decreases. Additionally, it is noted that the presence of roughness, characterized by the parameter c, prolongs the squeezing process duration compared to the smooth case (where $c = 0$).

The permeability parameter has the effect of reducing the squeezing duration for both rough and smooth surfaces. Furthermore, as the permeability parameter (Ψ) increases, the squeezing time consistently decreases.

D. Estimation of relative percentage of workload R_W and R_T squeeze film time

The relative percentage of R_W and R_T is defined as $R_W = \{\frac{W_{withroughness} - W_{withoutroughness}}{W_{withoutroughness}} \times 100\}$ and $R_T = \{\frac{T_{withroughness} - T_{withoutroughness}}{T_{withoutroughness}} \times 100\}$.

TABLE V: Variation of R_W and R_T for different values of c with $N = 0.5$, $M = 5$, $L = 0.15$ and $\Psi = 0.001$

Roughness Parameter	R_W		R_T	
	Azimuthal	Radial	Azimuthal	Radial
$c = 0.1$	4.49	4.05	1.75	-0.61
$c = 0.2$	5.67	3.91	7.55	-2.39
$c = 0.3$	7.75	3.67	19.35	-5.18

The data presented in Table V indicates with the rise in the value of roughness parameter (c), the azimuthal values of R_W and R_T rises considerably. On the other hand the values of radial roughness drops for a similar situation. This variation of rise and drop in the roughness pattern can be attributed to the following physical appearance. For the case of azimuthal roughness pattern, the rough striations take the shape of ridges and valleys oriented along the y-direction. This configuration obstructs the lubricant flow. Conversely, the radial roughness pattern features rough striations forming ridges and valleys along the x-direction, allowing the lubricant to escape more effortlessly. This leads to the rise and fall of the data in azimuthal and radial directions respectively.

V. Conclusion

The influence of squeezing action on micropolar fluid in the presence of an externally applied magnetic field is considered in this article. The basic for this fluid model was developed by Eringen, which is applied to the considered geometry of triangular plates, which are rough in nature and are backed by a porous facing at the lower surface. The pressure distribution is obtained by solving the Reynolds equation and the load-carrying capacity is obtained by integrating the pressure over the film region. The workload is intensified by the application of MPF as a lubricant, which is characterized by the coupling number N and the fluid clearance gap L. The induced magnetic field enhances the workload in contrast to the non-magnetic scenario of a similar situation. The presence of porosity reduces the workload, while the effect of surface roughness increases the workload compared to the smooth case by 7.75%, as illustrated in Table V. Additionally, it is observed that the squeeze time increases with higher values of the coupling number N, clearance gap L, Hartmann number M, in comparison to the non-magnetic case, and with the roughness parameter c, in comparison to the smooth case, by 19.35%. By considering the above observations an ideal bearing lubricant can maximize the performance of the plate.

References

[1] S. M. Anncy, T. Joseph, and S. Pranesh, "Linear and non-linear analyses of double diffusive chandrasekhar convection with heat and concentration source in micropolar fluid with saturated porous media under gravity modulation," *IAENG International Journal of Applied Mathematics*, vol. 50, no. 2, pp 342-358, 2020.

[2] H. Christensen and K. Tonder, Parametric Study and Comparison of Lubrication Models, *SINTEF*, 1969.

[3] T. G. Cowling, "Magnetohydrodynamics,"*Crane, Russak and Company, Inc., New York*, 1976.

[4] F. M. Elniel, S. Mustafa, A. Bahar, Z. A. Aziz, and F. Salah, "Effects of shear stress on magnetohydrodynamic (mhd) powell eyring fluid over a porous plate: A lift and drainage problem," *IAENG International Journal of Applied Mathematics*, vol. 51, no. 4, pp 851-860, 2021.

[5] A. C. Eringen, "Theory of micropolar fluids," *Journal of mathematics and Mechanics*, pp 1-18, 1966.

[6] S. T. Fathima, N. Naduvinamani, B. Hanumagowda, and J. S. Kumar, "Modified reynolds equation for different types of finite plates with the combined effect of mhd and couple stresses," *Tribology Transactions* , vol. 58, no. 4, pp 660–667, 2015.

[7] E. Hamza, "The magnetohydrodynamic squeeze film," *International Centre for Theoretical Physics*, Tech. Rep., 1987.

[8] B. Hanumagowda, B. Raju, J. Santhosh Kumar, and K. Vasanth, "Combined effect of surface roughness and pressure-dependent viscosity over couple-stress squeeze film lubrication between circular stepped plates," *Proceedings of the Institution of Mechanical Engineers, Part J: Journal of Engineering Tribology*, vol. 232, no. 5, pp 525-534, 2018.

[9] B. Halambi and H. BN, "Micropolar squeeze film lubrication analysis between rough porous elliptical plates and surface roughness effects under the MHD," *Ilkogretim Online*, vol. 20, no. 4, 2021.

[10] B. Hanumagowda, N. Chaithra, H. Doreswamy, and A. Salma, "Combined effect of surface roughness and micropolar fluids on squeeze film characteristics between rough flat plate and curved annular plates," *Malaya Journal of Matematik* (MJM), vol. 8, no.2, pp 570-575, 2020.

[11] D. C. Kuzma, "Magnetohydrodynamic squeeze films," 1964.

[12] I. Nayak, "Numerical study of mhd flow and heat transfer of an un steady third grade fluid with viscous dissipation," *IAENG International Journal of Applied Mathematics*, vol. 49, no. 2, pp 245-252, 2019.

[13] N. Naduvinamani and A. Siddangouda, "Combined effects of surface roughness and couple stresses on squeeze film lubrication between porous circular stepped plates," *Proceedings of the Institution of Mechanical Engineers, Part J: Journal of Engineering Tribology*, vol. 221, no. 4, pp 525-534, 2007.

[14] N. Naduvinamani, B. Hanumagowda, and S. T. Fathima, "Combined effects of mhd and surface roughness on couple-stress squeeze film lubrication between porous circular stepped plates," *Tribology inter national*, vol. 56, pp 19-29, 2012.

[15] J. Prakash and P. Sinha, "Squeeze film theory for micropolar fluids," ASME-AMER SOC MECHANICAL ENG, 1975.

[16] R. Patel, G. Deheri, and P. Vadher, "Performance of a magnetic fluid based squeeze film between transversely rough triangular plates," *Tribology in industry*, vol. 32, no. 1, p 33, 2010.

[17] J. Prakash and K. Tonder, "Roughness effects in circular squeeze plates," *ASLE TRANSACTIONS*, vol. 20, no. 3, pp 257-263, 1977.

[18] P. S. Rao, B. Murmu, and S. Agarwal, "Effects of surface roughness and non-newtonian micropolar fluid squeeze film between truncated conical bearings," *Journal of Nanofluids*, vol. 8, no. 6, pp 1338-1344, 2019.

[19] F. Salah and M. H. Elhafian, "Numerical solution for heat transfer of non-newtonian second-grade fluid flow over stretching sheet via successive linearization method," *IAENG International Journal of Applied Mathematics*, vol. 49, no. 4, pp 505-512, 2019.

[20] A. Siddangouda, "Squeezing film characteristics for micropolar fluid between porous parallel stepped plates," *Tribology in Industry*, vol. 37, no. 1, p 97, 2015.

[21] P. Sinha and C. Singh, "Micropolar squeeze films in porous hemispher ical bearings," *International Journal of Mechanical Sciences*, vol. 24, no. 8, pp 509-518, 1982.

[22] E. Sujatha, Sundarammal kesavan, "Combined effect of magneto hydrodynamics (MHD) and viscosity variation on triangular plates with couple stress fluid," *International Journal of Civil Engineering and Technology*, vol. 9, no. 6, 2018.

[23] A. Toloian, M. Daliri, and N. Javani, "The performance of squeeze film between parallel triangular plates with a ferro-fluid couple stress lubricant," *Advances in Tribology*, pp 1-8, 2020.

[24] P. A. Vadher, G. Deheri, and R. M. Patel, "Effect of transverse surface roughness on the performance of hydromagnetic squeeze film between conducting truncated conical plates," *Journal of Marine Science and Technology*, vol. 19, no. 6, p 12, 2011.